

Article

Design Framework for Motion Generation of Planar Four-Bar Linkage Considering Clearance Joints and Dynamics Performance

Xueao Liu ¹, Jianzhong Ding ^{1,*} and Chunjie Wang ²

¹ School of Mechanical Engineering and Automation, Beihang University, Beijing 100191, China; liuxueao@buaa.edu.cn

² State Key Laboratory of Virtual Reality Technology and Systems, Beihang University, Beijing 100191, China; wangcj@buaa.edu.cn

* Correspondence: jianzhongd@buaa.edu.cn

Abstract: In this paper, we present a novel design framework to connect linkage synthesis with dynamics performance of the linkage. The aim of the design framework is to improve the dynamics performance of the mechanism through linkage design, instead of improving manufacturing accuracy or changing driving strategy. Specifically, the design framework is to complete motion generation of four-bar linkage, considering clearance joints and dynamics performance. The constraint model of motion generation and the dynamics model of four-bar linkage are established, respectively. The coordinates of four joints of four-bar linkage are divided into two parts, one of parts is the parameters to improve the dynamics performance of the linkage and is selected as the optimization variables. The other parts of joint coordinates is to satisfy the kinematics requirements and is obtained by solving constraint equations of motion generation. Through optimization calculation, we can obtain the optimal configuration of the four-bar linkage that achieves specified task positions with high motion accuracy and low wear extent of clearance joint. Finally, a numerical example is proposed to demonstrate the novel design framework.



Citation: Liu, X.; Ding, J.; Wang, C. Design Framework for Motion Generation of Planar Four-Bar Linkage Considering Clearance Joints and Dynamics Performance.

Machines **2022**, *10*, 136. <https://doi.org/10.3390/machines10020136>

Academic Editor: Giuseppe Carbone

Received: 7 January 2022

Accepted: 9 February 2022

Published: 13 February 2022

Publisher's Note: MDPI stays neutral with regard to jurisdictional claims in published maps and institutional affiliations.



Copyright: © 2022 by the authors. Licensee MDPI, Basel, Switzerland. This article is an open access article distributed under the terms and conditions of the Creative Commons Attribution (CC BY) license (<https://creativecommons.org/licenses/by/4.0/>).

Keywords: linkage synthesis; motion generation; dynamics analysis; design framework; simulation-based design

1. Introduction

The task of linkage synthesis is to determine the link dimension to form the linkage that achieve the specified task positions. According to the past literature [1,2], linkage synthesis can be divided into three task specifications, namely, motion generation, function generation, and path generation. Generally, the methods of linkage synthesis include analytical method and optimization method. Analytical method is to derive the synthesis constraint equations and solve it to obtain the configuration of the linkage. McCarthy et al. [1], Freudenstein [3], and Wampler et al. [4] derived the constraint equations of four-bar linkages for motion generation, function generation, and path generation, respectively; additionally, see [5–7]. Plecnik et al. derived the constraint equations of six-bar linkage for motion generation [8], function generation [9], and path generation [10]. The advantage of analytical method is that all configurations of the linkage can be obtained by solving the constraint equations. The shortcoming is that it is difficult to solve the highly nonlinear polynomial equations. The optimization method is also a useful tool for linkage synthesis. The motion generation [11], path generation [12,13], and hybrid task generation [14] are studied by using different optimization algorithms. The advantage of the optimization method is that we do not need to formulate the constraint equations and it is easy to perform, but it is difficult to find the optimal configuration when the optimization variables are too many.

Many researchers have investigated the consideration of other performances during the initial stage of linkage design. Kiper et al. [15] studied the mixed problem of correlation of crank angles and dead-center design with function generation of planar four-bar linkage. Zhang et al. [16] presented a method to analyze the time-dependent kinematic reliability of four-bar linkage during the stage of function generation. Erkaya et al. [17] used neural–genetic optimization approach to design four-bar linkage for path generation simultaneously considering the joints clearance. El-Shakery et al. [18] presented a method to optimally synthesize links' lengths of four-bar linkage to achieve targeted transmission angle deviations. Daniali [19] proposed a design method to synthesize the path generation of four-bar linkage considering the joint clearance, and controlled the unwanted degrees of freedom by revising the mass distributions of the moving links. Bai [20] used optimization method to minimize the maximum absolute acceleration peaks of the mechanism through linkage dimension synthesis. In this paper, we present a novel design framework to synthesize the four-bar linkage for motion generation considering clearance joints and dynamics performance. Differently from the methods in the previous literature, the proposed design framework combines the analytical method for linkage synthesis and the optimization method for dynamics to obtain the optimal configuration of the linkage that completes the specified task positions with high motion accuracy and low wear extent of clearance joint.

Due to manufacturing error, the clearance is inevitable in the revolute joint of the linkage. The nonlinear impact between the journal and the bearing will reduce the operation accuracy and reliability of a mechanical system [21–23]. Dynamic modeling of the mechanism systems has been identified as an important tool in the analysis, design, optimization, and simulation. To establish the dynamic model and achieve the dynamics analysis of mechanical systems with clearance joints, scholars have presented many novel and effective methods, such as [24–28]. Based on the dynamic models, scholars around the world have carried out many significant research works about the dynamic response, performance evaluation, and optimization of mechanical systems with clearance joints. Flores [29] employed the dynamic model to study the effects of clearance size, driving velocity, and number of clearance joints on the dynamic response of mechanical systems, and evaluated the total computation time consumed in each simulation. Xiang et al. [30] employed the fractal method to evaluate the complexity of dynamic response of mechanisms with clearance joints. Li et al. [31] used the Monte Carlo method to analyze the kinematic accuracy and dynamic performance of a space deployable mechanism with joint clearance while considering parameter uncertainty. Considering clearance joints and uncertainties, Xiang et al. [32] proposed an analysis method for dynamic response and parameter sensitivity of mechanical systems based on Chebyshev polynomials method. Lai et al. [33] presented a prediction method of wear extent for clearance joints, and the method was validated by using experimental data. Wang et al. [34] studied the dynamic performance of a spatial parallel mechanism by dynamic simulation. However, the above research works have not improved the dynamic performance of the mechanical systems from the perspective of mechanism synthesis.

In this paper, the aim of the proposed design framework was to improve the dynamics performance during the stage of linkage synthesis. In the design framework, the constraint model of motion generation and the dynamics model of four-bar linkage were established, respectively. The coordinates of two fixed joints are the parameters to improve the dynamics performance of the linkage and were selected as the optimization variables, and the coordinates of two moving joints were to satisfy the kinematics requirements and are obtained by solving constraint equations of motion generation. Through optimization calculation, we can obtain the optimal configuration of the four-bar linkage that achieves specified task positions with high motion accuracy and low wear extent of clearance joint. In what follows, we demonstrate the performance of the design framework.

2. The Synthesis of Four-Bar Linkage for Motion Generation

Motion generation of four-bar linkage is widely used in engineering, for example, in the pick and place mechanism, car steering, walking robot, etc. The goal of motion

generation is to design four-bar linkages whose coupler link can pass the specified locations and orientations. For convenience, here, the above locations and orientations are called task positions. In this section, we use analytical method to derive the constraint equations of four-bar linkage for motion generation, and propose a strategy to check the kinematics performance of the obtained linkage.

2.1. Constraint Equation of Four-Bar Linkage for Motion Generation

Figure 1 shows the representation form of four-bar linkage for motion generation. Here, the task positions are P_i and $\theta_i, i = 0, \dots, m - 1$, where m denotes the maximum number of task positions that the linkage can arrive. The task positions are specified by designer. The task is to determine the coordinates of four joints (O, A, B and C) to form a four-bar linkage that can arrive the specified task positions.

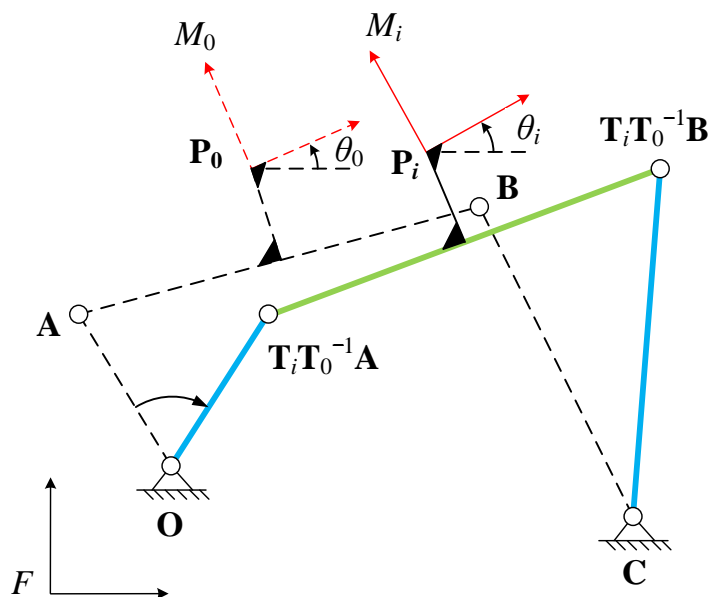


Figure 1. Four-bar linkage for motion generation.

In Figure 1, the four-bar linkage $OABC$ is moving from task position P_0 to P_i . Besides, OA is the crank, BC is the rocker, and AP_0B is the coupler link. The moving frame M_i is fixed on the coupler link, and its origin is at point P_i . The angle between the moving frame M_i and the initial frame F is the specified orientation angle θ_i . The homogeneous transformations from the moving frame M_i to the initial frame F can be given by the following:

$$T_i = \begin{bmatrix} \cos \theta_i & -\sin \theta_i & x_{P_i} \\ \sin \theta_i & \cos \theta_i & y_{P_i} \\ 0 & 0 & 1 \end{bmatrix} \tag{1}$$

where $(x_{P_i}, y_{P_i}, 1)^T$ denotes the coordinate of point P_i . Likewise, points O, A, B , and C can be denoted as $(x_O, y_O, 1)^T, (x_A, y_A, 1)^T, (x_B, y_B, 1)^T$, and $(x_C, y_C, 1)^T$ in the initial frame when the four-bar linkage is at the first position P_0 .

At first task position P_0 , we have the following constraint equation:

$$\begin{aligned} (A - O)^T(A - O) &= a^2, \\ (B - C)^T(B - C) &= c^2. \end{aligned} \tag{2}$$

where a and c are constants and denote the lengths of links OA and BC , respectively.

When the four-bar linkage arrives at the task position, P_i , the constraint equation can be expressed as follows:

$$\begin{aligned} (\mathbf{T}_i \mathbf{T}_0^{-1} \mathbf{A} - \mathbf{O})^T (\mathbf{T}_i \mathbf{T}_0^{-1} \mathbf{A} - \mathbf{O}) &= a^2, \\ (\mathbf{T}_i \mathbf{T}_0^{-1} \mathbf{B} - \mathbf{C})^T (\mathbf{T}_i \mathbf{T}_0^{-1} \mathbf{B} - \mathbf{C}) &= c^2. \end{aligned} \quad (3)$$

Then, we let Equation (3) subtract Equation (2) to eliminate a and c and obtain the constraint equations of four-bar linkage for motion generation, which are given as follows:

$$\begin{aligned} (\mathbf{T}_i \mathbf{T}_0^{-1} \mathbf{A} - \mathbf{O})^T (\mathbf{T}_i \mathbf{T}_0^{-1} \mathbf{A} - \mathbf{O}) - (\mathbf{A} - \mathbf{O})^T (\mathbf{A} - \mathbf{O}) &= 0, \\ (\mathbf{T}_i \mathbf{T}_0^{-1} \mathbf{B} - \mathbf{C})^T (\mathbf{T}_i \mathbf{T}_0^{-1} \mathbf{B} - \mathbf{C}) - (\mathbf{B} - \mathbf{C})^T (\mathbf{B} - \mathbf{C}) &= 0. \end{aligned} \quad (4)$$

In Equation (4), there are eight unknowns, which are the coordinates of four joints of the linkage. So the maximum number of task positions that the four-bar linkage can arrive is five. However, most cases in engineering are that the needed task positions is less than five [35]. This will allow some unknowns to be not constrained, and that can be the parameters for considering dynamics performance of the linkage.

2.2. Performance Verification of the Crank–Rocker Mechanism

After solving the synthesis constraint equations, the kinematics performance of obtained linkages need to be checked to obtain the non-defect linkages that can move in an orderly and smooth manner during the whole movement [36–38]. In this section, we mainly check whether the obtained linkages have the Grashof's defect, the order defect, the circuit defect, and the branch defect.

(1) Checking Grashof's defect:

Generally, we hope that the four-bar linkage has a crank that can fully rotate, so that the linkage can be driven by a continuously rotating motor. In this paper, we take the crank–rocker four-bar mechanism as the research object. All links lengths of the four-bar linkage can be obtained after the synthesis constraint equations are solved. As shown in Figure 2, a , b , c , and d denote the lengths of link \mathbf{OA} , \mathbf{AB} , \mathbf{BC} , and \mathbf{OC} , respectively.

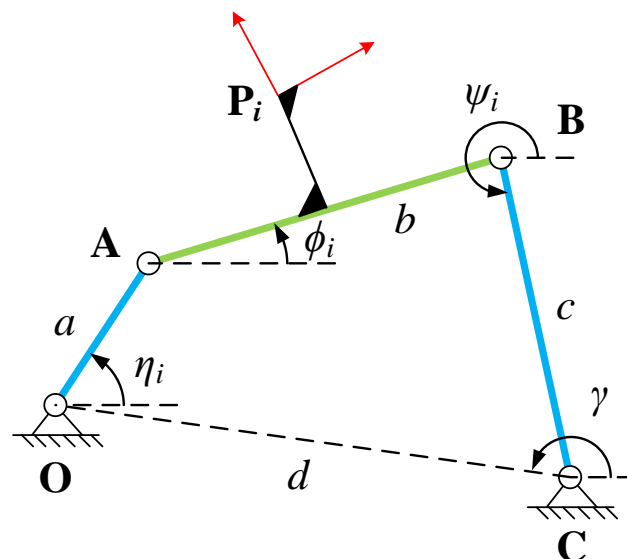


Figure 2. Four-bar linkage for kinematic performance verification.

For the crank–rocker mechanism, the link \mathbf{OA} is the input link and can rotate fully 360 degrees. According to Grashof's rule, a must be the length of the shortest link. Besides, let $L_{max} = \max \{b, c, d\}$. The linkage should also meet the constraint that the sum of a and L_{max} is less than the sum of the remaining two links lengths.

(2) Checking order defect:

When the input link rotates in one direction (clockwise or anticlockwise), the linkage arrives the task positions in an unspecified order, which means that the linkage has the

order defect. Here, we show a simple method to check the order defect. In Figure 2, $\eta_i, \phi_i, \psi_i, \gamma$ denote the angles of link **OA**, **AB**, **BC**, and **OC**, relative to x -axis of the initial frame when the linkage arrives at task position \mathbf{P}_i , and they can be determined after the candidate linkage are obtained. Then, we define the following:

$$\begin{cases} \mathbf{U}_i = [\cos \eta_i & \sin \eta_i & 0]^T \times [\cos \eta_{i+1} & \sin \eta_{i+1} & 0]^T \\ u_i = \text{sign}[\mathbf{U}_i(3)] \end{cases} \tag{5}$$

where operator “ \times ” denotes the cross product symbol, $\text{sign}[\bullet]$ represents sign function, and $\mathbf{U}_i(3)$ denotes the third component of vector \mathbf{U}_i . If u_i remains the same sign, it indicates that the linkage can orderly arrive the task positions when the crank rotates in clockwise or anticlockwise.

(3) Checking circuit defect and branch defect:

The linkage needs to be reassembled to move between two positions, which is called the circuit defect linkage. The linkage needs to pass through a singular configuration but needs not to be reassembled, which is called the branch defect linkage. To check the circuit defect and the branch defect, the motion state of each link should be identified when the input angle changes in the range of 360 degrees. So we establish the kinematic constraint equations, which are given as follows:

$$\begin{cases} f_1 : a \cos \eta + b \cos \phi + c \cos \psi + d \cos \gamma = 0, \\ f_2 : a \sin \eta + b \sin \phi + c \sin \psi + d \sin \gamma = 0. \end{cases} \tag{6}$$

In Equation (6), η is input variable, γ is constant, and ϕ and ψ are unknowns that should be solved. Because of the property of $\cos(\bullet)$ function, there are two sets of solutions of ϕ and ψ for a specified value of η . Here, we divide η into s parts in 360 degrees, which include m values of input angles for the linkage at m task positions. By substituting these s input angles into Equation (6) and solving them, we can obtain the following:

$$\begin{cases} \eta_1, [\phi_{11}, \psi_{11}], [\phi_{12}, \psi_{12}] \\ \eta_2, [\phi_{22}, \psi_{22}], [\phi_{21}, \psi_{21}] \\ \dots \\ \eta_j, [\phi_{j,1}, \psi_{j,1}], [\phi_{j,2}, \psi_{j,2}] \\ \dots \\ \eta_s, [\phi_{s,2}, \psi_{s,2}], [\phi_{s,1}, \psi_{s,1}] \end{cases} \tag{7}$$

In Equation (7), the index of each set of solution is disordered, this means that we do not know the linkage is at position $[\phi_{21}, \psi_{21}]$ or $[\phi_{22}, \psi_{22}]$ when the linkage moves from η_1 to η_2 . Here, we use Newton iteration method to sort the solutions into two branches. The Newton iteration equations of the linkage can be written as follows:

$$\begin{cases} [\phi_{j+1,1}, \psi_{j+1,1}]^T = [\phi_{j,1}, \psi_{j,1}]^T - \mathbf{J}^{-1}([\phi_{j,1}, \psi_{j,1}]) \mathbf{f}_{12}([\eta_{j+1}, \phi_{j,1}, \psi_{j,1}]) \\ [\phi_{j+1,2}, \psi_{j+1,2}]^T = [\phi_{j,2}, \psi_{j,2}]^T - \mathbf{J}^{-1}([\phi_{j,2}, \psi_{j,2}]) \mathbf{f}_{12}([\eta_{j+1}, \phi_{j,2}, \psi_{j,2}]) \end{cases} \tag{8}$$

where \mathbf{J} is the Jacobian matrix,

$$\mathbf{J} = \begin{bmatrix} -b \sin \phi & -c \sin \psi \\ b \cos \phi & c \cos \psi \end{bmatrix} \quad \text{and} \quad \mathbf{f}_{12} = [f_1, f_2]^T \tag{9}$$

Based on Equation (8), the positions $[\phi_{j+1,1}, \psi_{j+1,1}]$ and $[\phi_{j+1,2}, \psi_{j+1,2}]$ can be obtained from corresponding positions $[\phi_{j,1}, \psi_{j,1}]$ and $[\phi_{j,2}, \psi_{j,2}]$ when the linkage moves from η_1 to η_2 . Do $s - 1$ times for the above process, the solutions can be sorted into two separated branches, which can be denoted as follows:

$$\text{Branch1} = \begin{cases} \eta_1, [\phi_{11}, \psi_{11}] \\ \eta_2, [\phi_{21}, \psi_{21}] \\ \dots \\ \eta_j, [\phi_{j,1}, \psi_{j,1}] \\ \dots \\ \eta_s, [\phi_{s,1}, \psi_{s,1}] \end{cases}, \quad \text{Branch2} = \begin{cases} \eta_1, [\phi_{12}, \psi_{12}] \\ \eta_2, [\phi_{22}, \psi_{22}] \\ \dots \\ \eta_j, [\phi_{j,2}, \psi_{j,2}] \\ \dots \\ \eta_s, [\phi_{s,2}, \psi_{s,2}] \end{cases} \quad (10)$$

Then we test if m specified task positions are always on one of the two sorted branches. For example, Figure 3 shows that ϕ and ψ of all specified task positions are always on branch 1. If all specified task positions are on the same branch, we test the Jacobian determinants of the branch that all task positions are on. If the signs of the Jacobian determinants remain unchanged, the candidate linkage are non-defect linkage.

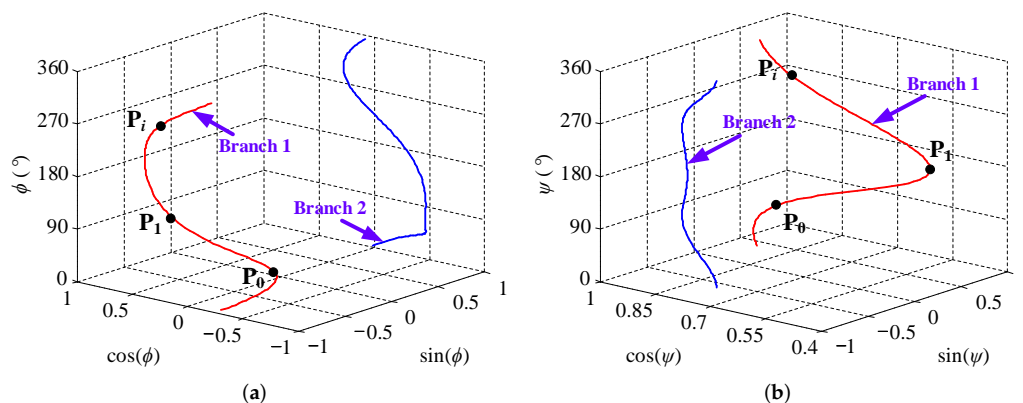


Figure 3. The m task positions are on the same branch. (a) All task angles of ϕ on branch 1. (b) All task angles of ψ on branch 1.

If the linkage has no Grashof’s defect, order defect, circuit defect and branch defect, the linkage can be selected as the desired crank–rocker mechanism that can pass through m task positions in an orderly and smooth manner.

3. Dynamics Modeling for Four-Bar Linkage with Revolute Clearance Joints

Generally, the links of four-bar linkage are interconnected by four revolute joints. For an ideal revolute joint, the center of journal always coincides with that of bearing in the whole motion process. In fact, the joint clearance is inevitable. When the joint clearance is considered in a revolute joint, it is obvious that the journal can move freely inside the bearing, and the nonlinear impact will occur between the journal and the bearing. Further, the above impact will exacerbate the wear between the journal and the bearing. Therefore, the existence of joint clearance will reduce the operation accuracy and service life of four-bar linkage. To study the dynamics characteristics of four-bar linkage with revolute clearance joints, we will establish its dynamics model in this section.

Figure 4 shows the configuration of a revolute joint with clearance.

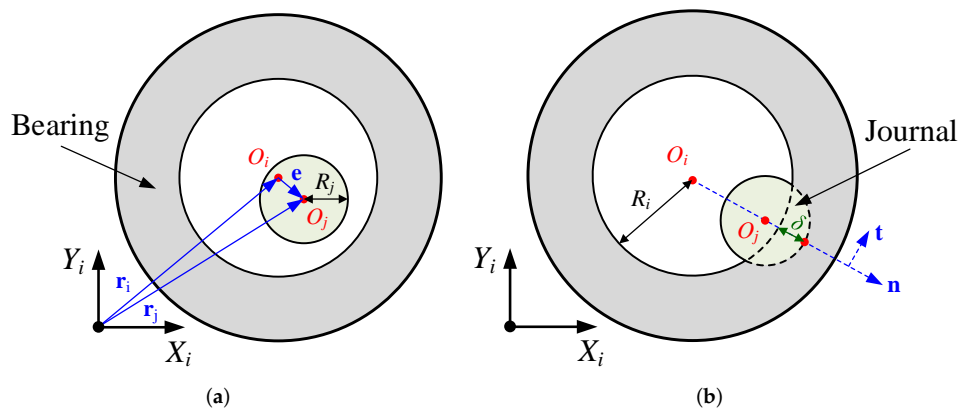


Figure 4. A revolute joint with clearance. (a) Separation status. (b) Contact status.

Specifically, the separation status refers to the state where the journal is not in contact with the bearing. The contact status refers to the state where the journal is in contact with the bearing. Here, the bearing is fixed on the body i , and the journal is fixed on the body j . In addition, $\{X_i, Y_i\}$ denotes the local coordinate system fixed on the body i . In this paper, the bearing and journal are both regarded as rigid bodies. Besides, O_i denotes the bearing center, and R_i denotes the bearing inside radius. O_j denotes the journal center, and R_j denotes the journal radius. Then, we let \mathbf{r}_i denote the position vector of O_i , relative to the origin of $\{X_i, Y_i\}$, \mathbf{r}_j denote the position vector of O_j relative to the origin of $\{X_i, Y_i\}$, and \mathbf{e} denote the position vector of O_j relative to O_i . According to the geometric relationship, we obtain the following:

$$\mathbf{e} = \mathbf{r}_j - \mathbf{r}_i. \tag{11}$$

We let c_R denote the radial clearance. According to the geometric relationship, we obtain the following:

$$c_R = R_i - R_j. \tag{12}$$

Further, the penetration depth between the journal and the bearing can be expressed as follows:

$$\delta = \begin{cases} 0, & |\mathbf{e}| \leq c_R \\ |\mathbf{e}| - c_R, & |\mathbf{e}| > c_R \end{cases} \tag{13}$$

When $|\mathbf{e}|$ is not equal to 0, the unit vector in the direction of \mathbf{e} is denoted as \mathbf{n} , and we obtain the following:

$$\mathbf{n} = \frac{\mathbf{e}}{|\mathbf{e}|}. \tag{14}$$

The orthogonal unit vector of \mathbf{n} is denoted as \mathbf{t} , and we obtain it by rotating \mathbf{n} anti-clockwise by 90° . When the journal is in contact with the bearing, the position vector of contact point relative to O_i is denoted as \mathbf{r}_c , and its expression is the following:

$$\mathbf{r}_c = \mathbf{e} + R_j \mathbf{n}. \tag{15}$$

The normal velocity of the contact point is denoted as v_n , and the tangential velocity of the contact point is denoted as v_t . According to the motion relationship, v_n and v_t can be expressed as follows:

$$\begin{cases} v_n = \dot{\delta} = \dot{\mathbf{r}}_c \mathbf{n}, \\ v_t = \dot{\mathbf{r}}_c \mathbf{t}. \end{cases} \tag{16}$$

When the journal is in contact with the bearing, the contact force can be divided into the normal force and the tangential force. The direction of the normal force is along the direction of \mathbf{n} , and the direction of the tangential force is along the direction of \mathbf{t} . In this paper, the normal force is described by using the Lankarani–Nikravesh contact force model [39], and the tangential force is described by using the modified Coulomb

friction model [22]. The above two models are widely used for the dynamics modeling of mechanical systems with clearance joints. According to Reference [39], the normal force is expressed as follows:

$$F_n = K\delta^n + D\dot{\delta}. \quad (17)$$

In Equation (17), n denotes the nonlinear exponent, and it equals 1.5 here. Besides, K denotes the stiffness coefficient, and its expression is as follows:

$$K = \frac{4}{3(\sigma_i + \sigma_j)} \sqrt{\frac{R_i R_j}{R_i - R_j}}. \quad (18)$$

where σ_i and σ_j denote the material parameters. In this paper, the expressions of σ_i and σ_j are as follows:

$$\sigma_i = \sigma_j = \frac{1 - \rho^2}{\pi E}. \quad (19)$$

where E denotes the Young's modulus and ρ denotes the Poisson's ratio. In Equation (17), D denotes the damping coefficient, and its expression is as follows:

$$D = \frac{3K(1 - c_e^2)\delta^n}{4\dot{\delta}^{(-)}}. \quad (20)$$

where c_e and $\dot{\delta}^{(-)}$ denote the restitution coefficient and the initial impact velocity, respectively. According to Reference [22], the tangential force is expressed as follows:

$$F_t = \mu F_n. \quad (21)$$

where μ denotes the friction coefficient, and we obtain the following:

$$\mu = \begin{cases} \mu_s \sin \frac{\pi|v_t|}{2V_s}, & |v_t| < V_s \\ \frac{\mu_d + \mu_s}{2} + \frac{1}{2}(\mu_s - \mu_d) \cos \left(\pi \frac{|v_t| - V_s}{V_d - V_s} \right), & V_s \leq |v_t| \leq V_d \\ \mu_d, & |v_t| > V_d \end{cases} \quad (22)$$

In Equation (22), μ_s denotes the static friction coefficient, μ_d denotes the sliding friction coefficient, V_s denotes the stick–slip switch velocity, and V_d denotes the static–sliding switch velocity.

In this research work, the dynamic modeling method was not our research focus. For convenience, we employ the MSC.ADAMS software to establish the dynamics model of four-bar linkage with clearance joints. In MSC.ADAMS software, the dynamics equations of multibody system are established by using the Lagrange equation, and the specific principle has been presented in reference [40]. At present, MSC.ADAMS has been widely used for dynamics simulation of mechanical systems with clearance joints. Through the secondary development of MSC.ADAMS software, the contact force model of clearance joint is established by using Equations (11) and (22). Besides, the dynamics model of four-bar linkage is solved by using the wstiff-SI2 integrator algorithm, whose principle has been specifically introduced in Reference [41].

4. Design Framework for Motion Generation of Four-Bar Linkage

Traditionally, the synthesis of four-bar linkage for motion generation can only let the obtained mechanism pass through the specific task positions, and its dynamics performance is generally not concerned. As mentioned above, if the number of task positions is less five, parts of joints coordinates can be used as the design parameters for considering dynamics performance of the linkage. Here, the dynamics performance refers to the performance that should be evaluated by dynamics analysis. Because of the inevitable joint clearance, the actual operating state of the four-bar linkage will be different from the ideal one. Therefore, when carrying out the synthesis of four-bar linkage for motion generation, we

need to consider the dynamics performance, which will make the result have more practical engineering significance. After the dynamics model of four-bar linkage is established, we can use it to evaluate the dynamics performance. Next, combining the dynamics model and the synthesis method of Section 2, we will propose a design framework for motion generation of four-bar linkage considering clearance joints and dynamics performance.

4.1. Dynamics Performance Evaluation

In this paper, the dynamics performance of four-bar linkage includes the operation accuracy and the wear extent of clearance joint, which can be analyzed by dynamics simulation. According to Section 2, the output link should pass through several specific positions during the motion process. If the four-bar linkage operates continuously, the output link needs to pass through the specific position at the specific time. It should be noticed that the output link also needs to follow the specific orientation when passing through the specific position. Therefore, the operation accuracy can be subdivided into the position accuracy and the orientation accuracy. The evaluation parameter of position accuracy is expressed as follows:

$$e_p = \sqrt{\sum [(x_D^{(i)} - x_I^{(i)})^2 + (y_D^{(i)} - y_I^{(i)})^2]}. \quad (23)$$

where $(x_D^{(i)}, y_D^{(i)})$ denotes the actual position that the output link passes through at the i th specific time, and $(x_I^{(i)}, y_I^{(i)})$ denotes the corresponding ideal position. $(x_D^{(i)}, y_D^{(i)})$ is obtained by dynamics simulation. Besides, the evaluation parameter of orientation accuracy is expressed as follows:

$$e_a = \sqrt{\sum (\theta_D^{(i)} - \theta_I^{(i)})^2}. \quad (24)$$

where $\theta_D^{(i)}$ denotes the actual orientation of output link at the i th specific time, and $\theta_I^{(i)}$ denotes the corresponding ideal orientation. $\theta_I^{(i)}$ is obtained by dynamics simulation. The smaller the e_p and e_a , the higher the operation accuracy of four-bar linkage.

In fact, the wear extent of clearance joint directly determines the service life of four-bar linkage. In this paper, we employ the Archard model to describe the wear extent of clearance joint [42]. The Archard model can be expressed as follows:

$$V = \frac{k}{H} F_n s_d. \quad (25)$$

where k and H denote the material related coefficients, s_d denotes the relative slip distance between the journal and the bearing, and V denotes the wear volume. During the dynamics simulation, s_d is difficult to obtain directly. After differentiating Equation (25) relative to time, we can obtain the following:

$$\frac{dV}{dt} = \frac{k}{H} F_n |v_t|. \quad (26)$$

Then, we obtain the following:

$$V = \frac{k}{H} \int F_n |v_t| dt. \quad (27)$$

Generally, k and H are constant, so the evaluation parameter of wear extent of clearance joint can be expressed as follows:

$$w_A = \int F_n |v_t| dt. \quad (28)$$

In this paper, we will set a shorter operating time span for four-bar linkage, so the effect of wear on F_n and v_t can be neglected. The smaller the w_A , the lighter the wear extent of clearance joint.

4.2. The Novel Design Framework

In this section, we will propose a design framework for motion generation of four-bar linkage considering clearance joints and dynamics performance. The novel design framework covers the mechanism synthesis method, dynamics simulation method, and multi-objective optimization method, and its flowchart is shown in Figure 5.

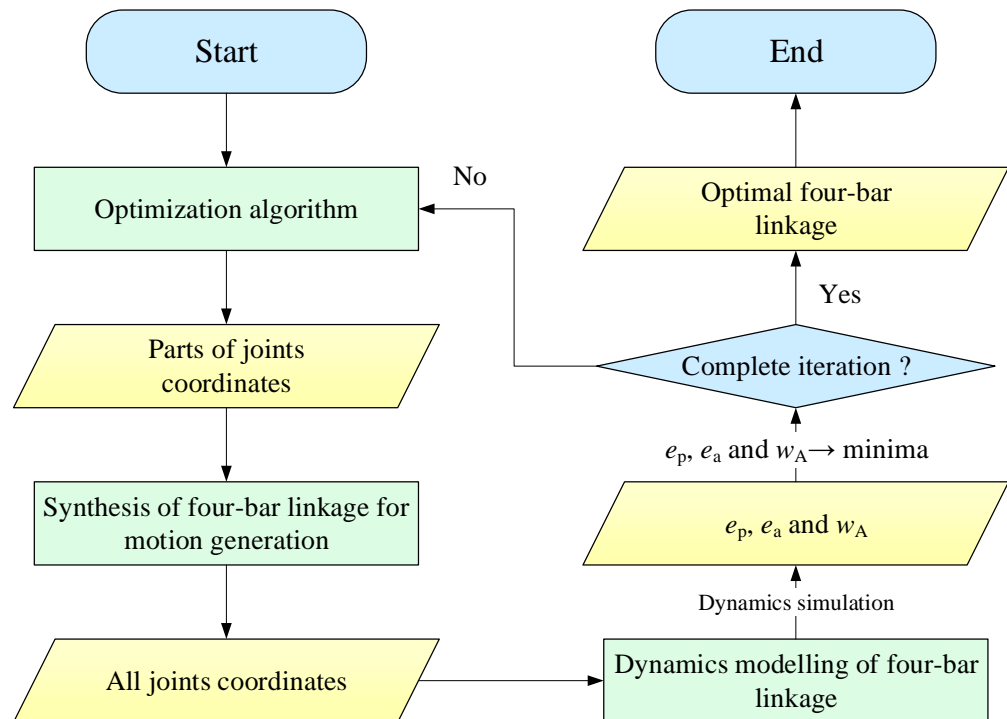


Figure 5. Flowchart of design framework.

First, the optimization algorithm generates parts of joints coordinates of four-bar linkage based on the number of task positions. Then, these coordinates are used for carrying out the synthesis of four-bar linkage for motion generation, and all joints coordinates are obtained. Using the above joints coordinates, we can establish the dynamics model of four-bar linkage. After dynamics simulation, e_p , e_a and w_A can be calculated. Here the optimization objective is to minimize e_p , e_a and w_A simultaneously. When the optimization iteration calculation is completed, we can obtain the Pareto optimal set of the joints coordinates for optimization variables. Meanwhile, the optimal joints coordinates of four-bar linkage are also obtained. Finally, we can determine the optimal four-bar linkage.

In this paper, we employ the non-dominated sorting genetic Algorithm II (NSGA-II) to solve the above multi-objective optimization problem. The principle of NSGA-II has been specifically introduced in reference [43]. Of course, the usage of NSGA-II is just an example, and other effective algorithms can also be used for solving the above multi-objective optimization problem. To sum up, the optimization mathematical model is expressed as follows:

$$\begin{cases} \min & e_p, e_a, w_A. \\ \text{s.t.} & x_O^L \leq x_O \leq x_O^U, \\ & y_O^L \leq y_O \leq y_O^U, \\ & x_C^L \leq x_C \leq x_C^U, \\ & y_C^L \leq y_C \leq y_C^U. \end{cases} \tag{29}$$

where (x_O, y_O) and (x_C, y_C) denote the frame coordinates of four-bar linkage, $x_O^L, y_O^L, x_C^L,$ and y_C^L denote the lower limits of $x_O, y_O, x_C,$ and $y_C,$ respectively, and $x_O^U, y_O^U, x_C^U,$ and y_C^U denote the upper limits of $x_O, y_O, x_C,$ and $y_C,$ respectively. It should be noticed that all objective functions are closely related to the clearance joints. If the joint clearance does not exist, all objective functions will always equal 0. Therefore, the joint clearance must have an obvious effect on the optimization results. In order to reduce the computational complexity, we only consider only one clearance joint in the following research works, which is same as reference [20]. Of course, the proposed method has certain generality, and designers can carry out the optimization calculation considering the multiple clearance joints.

5. Case Study

In this section, we will give an example to demonstrate the design framework proposed by us. For the motion generation of four-bar linkage, we let the output link pass through three specific task positions during the motion process, and select two fixed joints coordinates as optimization variables for considering dynamics performance. Besides, the output link also needs to follow the specific orientation when passing through the specific position. The targeted positions and orientations are shown in Table 1.

Table 1. The targeted positions and orientations.

No.	Position (m)	Orientation (°)
1	(0, 0)	0
2	(−0.61, 0.22)	−20
3	(0.48, 0.87)	−40

Here, we set the time when the output link is at position 1 as the initial time. Besides, we let the output link pass through positions 1–3 in turn.

In the dynamics model, the four-bar linkage consists of three ideal revolute joints, one between the crank and the frame, one between the crank and the output link, and the other between the rocker and the frame, and a revolute clearance joint between the output link and the rocker. The crank is driven by using the constant angular velocity 100 °/s. The mass parameters values of the four-bar linkage are shown in Table 2.

Table 2. The mass parameters values of the four-bar linkage.

Body	Mass (kg)	Moment of Inertia (kg · m ²)
Crank	2 OA	0.04 OA ²
Output link	1.25 AB	0.05 AB ²
Rocker	1.1 BC	0.0124 BC ²

In addition, the related parameters values of contact force model are shown in Table 3.

At the initial time, we let the centers of the journal and bearing be coincident. Besides, the total simulation time is set to 7.2 s, which means that the crank will rotate 2 turns. Therefore, in fact, there will be six targeted positions and orientations given by the following:

$$\begin{cases} (x_I^{(1)}, y_I^{(1)}, \theta_I^{(1)}) = (0, 0, 0), \\ (x_I^{(2)}, y_I^{(2)}, \theta_I^{(2)}) = (-0.61, 0.22, -20), \\ (x_I^{(3)}, y_I^{(3)}, \theta_I^{(3)}) = (0.48, 0.87, -40), \\ (x_I^{(4)}, y_I^{(4)}, \theta_I^{(4)}) = (0, 0, 0), \\ (x_I^{(5)}, y_I^{(5)}, \theta_I^{(5)}) = (-0.61, 0.22, -20), \\ (x_I^{(6)}, y_I^{(6)}, \theta_I^{(6)}) = (0.48, 0.87, -40). \end{cases} \tag{30}$$

During the dynamics simulation, the related parameters values of wstiff-SI2 integrator algorithm are shown in Table 4.

Table 3. The related parameters values of contact force model.

Parameter	Value	Parameter	Value
n	1.5	c_e	0.95
ρ	0.3	μ_s	0.04
E	69 Gpa	μ_d	0.03
R_i	7.02 mm	V_s	10^{-3} m/s
R_j	7 mm	V_d	1.5×10^{-3} m/s

Table 4. The related parameters values of wstiff-SI2 integrator algorithm.

Parameter	Value	Parameter	Value
Output step size	2×10^{-5}	Minimum step size	10^{-11}
Maximum order	12	Local truncation error	$<10^{-8}$

In this paper, the parameter configuration of NSGA-II is shown in Table 5.

Table 5. Parameter configuration of NSGA-II.

Population Size	Number of Generation	Crossover Probability	Crossover Index	Mutation Index
12	20	0.9	10	20

Besides, the limits of optimization design variables are shown in Table 6.

Table 6. The limits of optimization design variables.

$x_O^L(m)$	$x_C^L(m)$	$x_O^U(m)$	$x_C^U(m)$	$y_O^L(m)$	$y_C^L(m)$	$y_O^U(m)$	$y_C^U(m)$
-1	0	1	3	-2	-1	0	1

After optimization calculation, we obtain the Pareto optimal set shown in Table 7.

Table 7. The Pareto optimal set.

No.	$x_O(m)$	$y_O(m)$	$x_C(m)$	$y_C(m)$	$e_p (\times 10^{-2} \text{ mm})$	$e_a (\times 10^{-3} \text{ }^\circ)$	$w_A(Nm)$
1	-0.99	-0.21	1.28	0.68	2.05	0.98	5.80
2	-0.87	-0.18	1.26	0.68	2.05	1.03	3.16
3	-0.90	-1.82	0.73	0.93	3.22	0.40	1.16
4	0.22	-1.81	0.73	0.96	2.06	0.47	0.45
5	-0.00	-1.82	0.73	0.96	2.63	0.62	0.33
6	0.08	-1.80	0.73	0.96	3.94	0.85	0.26
7	-0.90	-1.96	0.75	0.93	3.59	0.37	0.83
8	0.48	-0.68	0.72	0.93	7.52	3.68	0.15
9	-0.90	-1.82	0.73	0.93	3.33	0.35	1.73
10	0.08	-1.80	0.73	0.96	3.94	0.85	0.26
11	-0.90	-1.82	0.73	0.93	3.23	0.39	1.18
12	0.21	-1.82	0.73	0.96	2.48	0.60	0.44
13	0.08	-1.80	0.73	0.97	3.08	0.71	0.26
14	0.48	-0.67	0.72	0.93	6.69	3.46	0.15

Here, we independently execute the above optimization three times, and the obtained Pareto optimal solutions are relatively steady, which means that the parameter configu-

ration of NSGA-II is rational. In addition, it takes 12 h to complete a single optimization calculation.

6. Results and Discussions

Table 7 illustrates that the three optimization objectives, e_p , e_a and w_A , are contradictory, which means they can not reach the minimum simultaneously in a configuration. So, we select three solutions from the Pareto optimal set to carry out the further research. The three solutions have the minimum e_p , the minimum e_a , and the minimum w_A , which are No. 1, No. 9, and No. 8, respectively. According to the synthesis constraint, the coordinates of all joints for three selected configurations can be obtained and are shown in Table 8.

Table 8. The joints coordinates for three selected configurations.

No.	Joint O	Joint A	Joint B	Joint C
1	(−0.99, −0.21)	(−0.88, −1.05)	(0.22, 1.92)	(1.28, 0.68)
9	(−0.90, −1.82)	(−0.36, −2.72)	(2.02, −0.69)	(0.72, 0.93)
8	(0.48, −0.67)	(0.94, −0.72)	(1.97, −0.64)	(0.72, 0.93)

The specific configurations can be determined based on the joints coordinates. For the three configurations, we carry out the kinematics simulation, and obtain the motion processes of four-bar linkages. Figure 6 shows the motion process of the four-bar linkage for the configuration of the minimum e_p , Figure 7 shows the motion process of the four-bar linkage for the configuration of the minimum e_a and Figure 8 shows the motion process of the four-bar linkage for the configuration of the minimum w_A . Through the motion process, the four-bar linkages for the three configurations can pass through the task positions in an orderly and smooth manner.

In an actual engineering application, we can manufacture the output part of the output link by using the materials with lower quality, such as carbon fiber. Therefore, the effect of the output part on the inertia properties of the whole link can be neglected. Then, for three configurations, we carry out the dynamics simulation, and obtain the variation curves of output position, output orientation, and $F_n \cdot |v_t|$, which are shown in Figures 9–11.

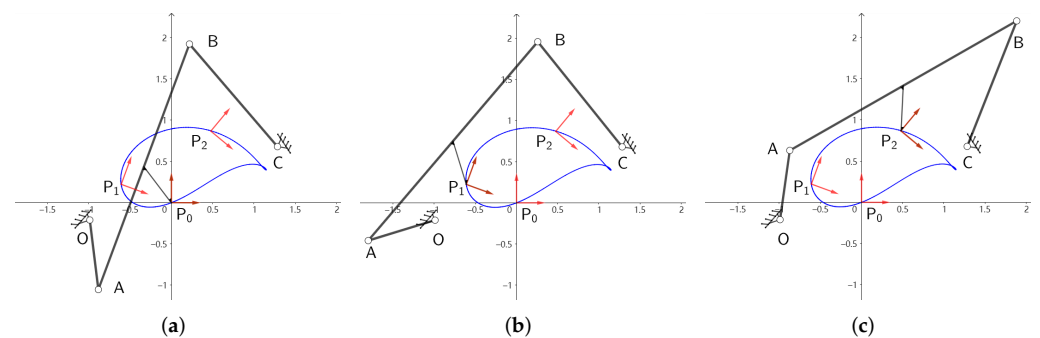


Figure 6. The motion process of the four-bar linkage for the configuration of the minimum e_p . (a) Task position 1. (b) Task position 2. (c) Task position 3.

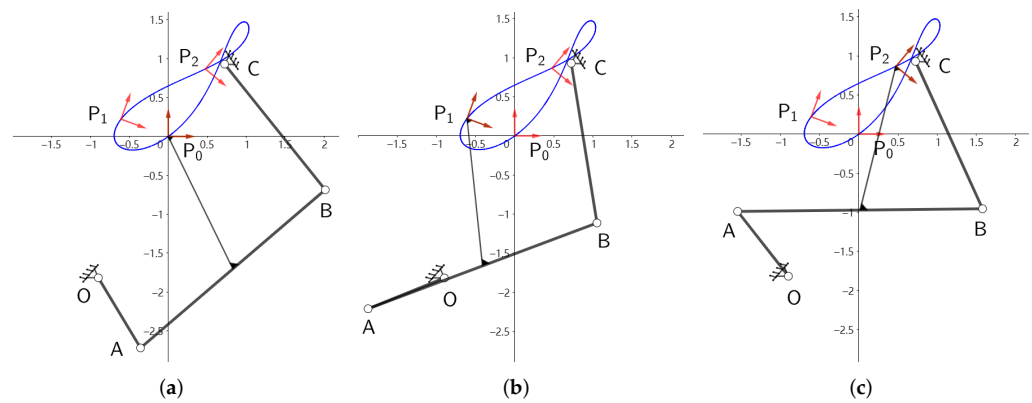


Figure 7. The motion process of the four-bar linkage for the configuration of the minimum e_a . (a) Task position 1. (b) Task position 2. (c) Task position 3.

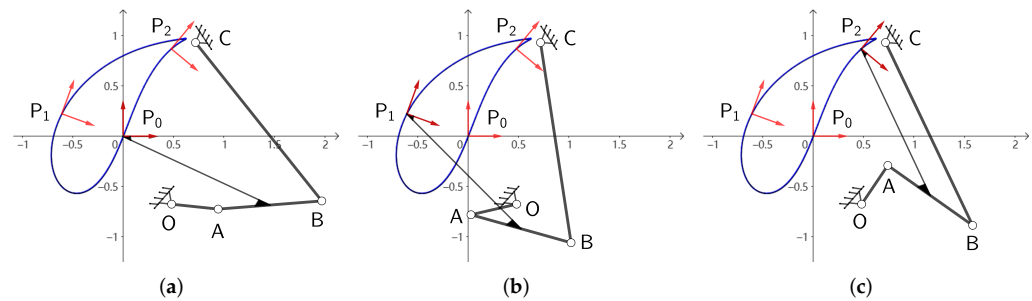


Figure 8. The motion process of the four-bar linkage for the configuration of the minimum w_A . (a) Task position 1. (b) Task position 2. (c) Task position 3.

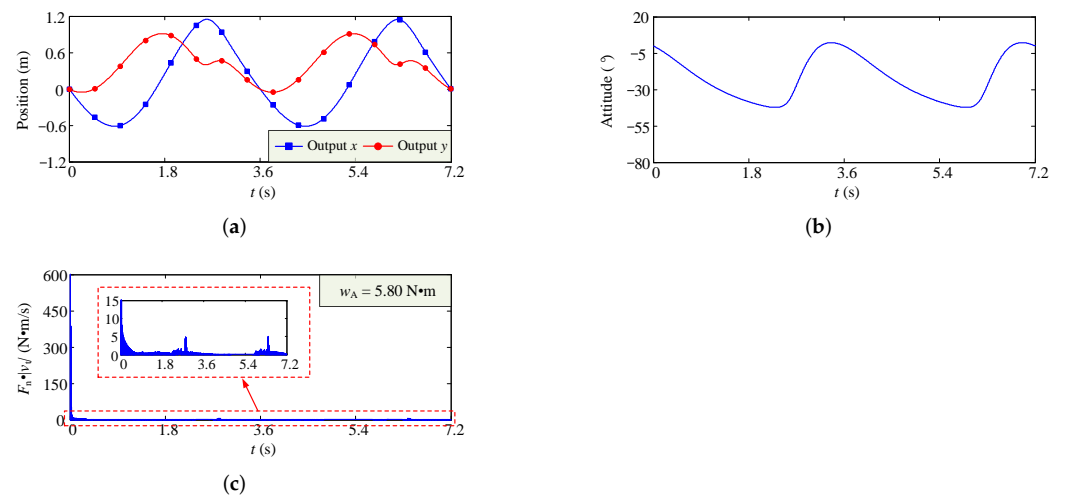


Figure 9. The results of dynamics simulation for the configuration of the minimum e_p . (a) Variation curves of output position. (b) Variation curve of output orientation. (c) Variation curve of $F_n \cdot |v_t|$.

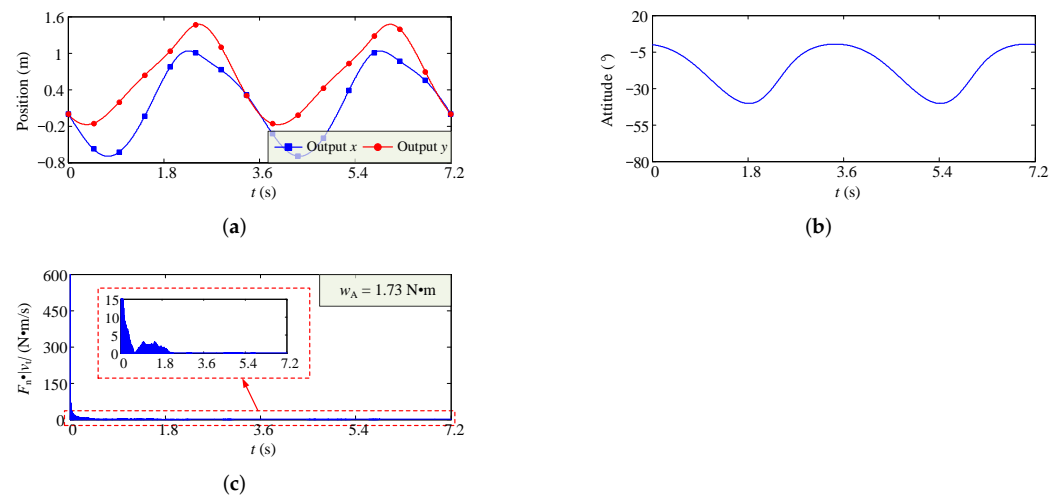


Figure 10. The results of dynamics simulation for the configuration of the minimum e_a . (a) Variation curves of output position. (b) Variation curve of output orientation. (c) Variation curve of $F_n \cdot |v_t|$.

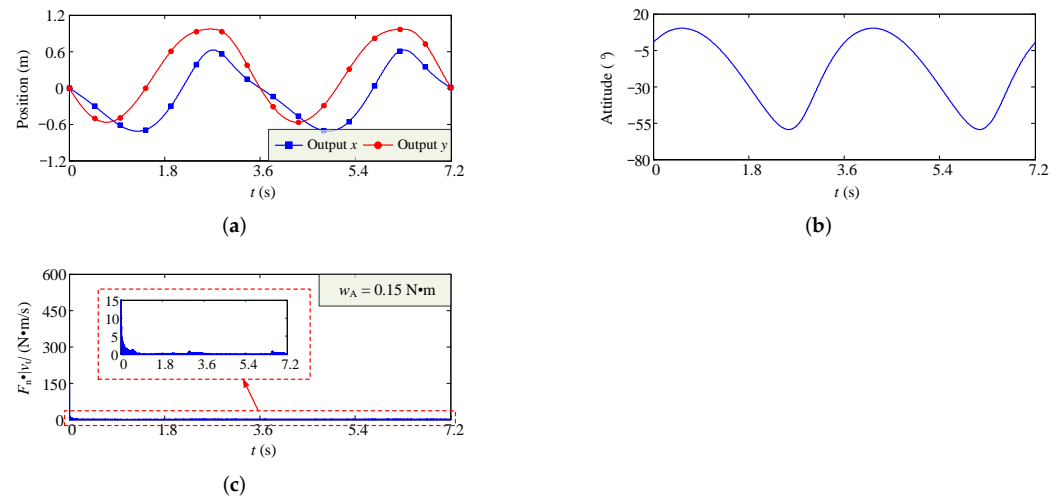


Figure 11. The results of dynamics simulation for the configuration of the minimum w_A . (a) Variation curves of output position. (b) Variation curve of output orientation. (c) Variation curve of $F_n \cdot |v_t|$.

Figures 9–11. show that the motion of four-bar linkage is relatively stable, and the wear of clearance joint is more severe when the four-bar linkage begins to move.

The above analysis results also show that the values of e_p and e_a are small, which means that the operation accuracy of the mechanism is relatively easy to guarantee. In actual engineering application, the wear extent of clearance joint directly determines the service life of four-bar linkage. In view of this, we select the solution with the minimum w_A from the Pareto optimal set as the final optimal solution.

To validate the proposed design framework, we compare it with the traditional linkage synthesis method [44]. In traditional linkage synthesis method, this is the motion generation for three task positions. The common strategy is that giving the specified values for unconstrained parameters or random selecting values in the corresponding ranges. Here, we randomly select 1000 groups of values for the parameters x_O , y_O , x_C , and y_C in their ranges, and select the non-defect configuration with minimum wear extent, w_A . The joints coordinates of selected four-bar linkage are shown in Table 9. Furthermore, Figure 12 shows the linkage can pass through the three task positions in an orderly and smooth manner. Then, for this configurations, we carry out the dynamics simulation, and obtain the variation curves of output position, output orientation and $F_n \cdot |v_t|$, which are shown in Figure 13. For this configuration, the wear extent $w_A = 14.84$ Nm, which is greater than the

wear extent of the configuration obtained by the design framework. The above research works illustrate that the design framework is reliable and can be considered for engineering practice.

Table 9. The joints coordinates of the configuration obtained by traditional linkage synthesis method.

Joint O	Joint A	Joint B	Joint C
(−0.44, −0.63)	(−0.06, −1.16)	(2.20, −0.85)	(0.75, 0.92)

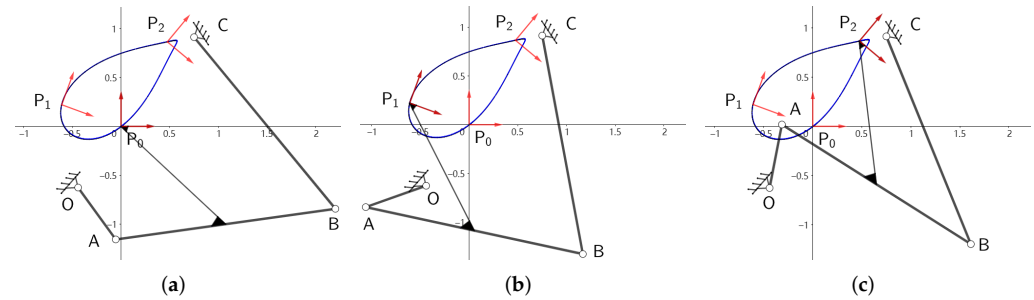


Figure 12. The motion process of the four-bar linkage for the configuration obtained by traditional linkage synthesis method. (a) Task position 1. (b) Task position 2. (c) Task position 3.

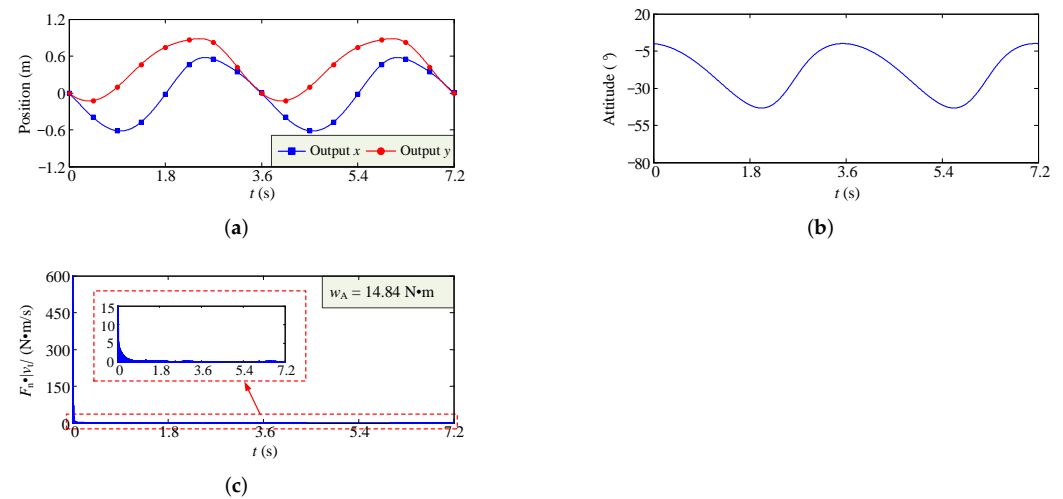


Figure 13. The results of dynamics simulation for the configuration obtained by traditional linkage synthesis method. (a) Variation curves of output position. (b) Variation curve of output orientation. (c) Variation curve of $F_n \cdot |v_t|$.

7. Conclusions

In this paper, we present a novel design framework for motion generation of planar four-bar linkage, especially considering the effect of joint clearance on the dynamics performance of the linkage. For the novel design framework, the mechanism synthesis and dynamics analysis methods are connected by multi-objective optimization theory, which has not been reported before. Through the novel design framework, designers could obtain the planar four-bar linkages that better meet the actual engineering requirements. To demonstrate the design framework, this paper gives a numerical example for designing a four-bar linkage that can pass through three specified task positions in an orderly and smooth manner. Specifically, the NSGA-II and analytical constraint model are employed to determine the optimal coordinates of two fixed joints that can make the linkage has the higher operation accuracy and the lower joint wear extent. Simulation results illustrate that the cumulative position and attitude errors caused by joint clearance are smaller than

0.1 mm and 0.01° , respectively, which means that the operation accuracy of linkage is relatively easy to guarantee. Therefore, we select the solution with the minimum joint wear extent to determine the final configuration of the linkage. Dynamics simulation results illustrate that the obtained linkage can satisfy the requirements of kinematics and dynamics simultaneously, which verifies the effectiveness of the design framework. Besides, the number of joints coordinates for kinematics and dynamics can be changed according to the number of specified task positions. Furthermore, the design framework can be extended to six-bar and eight-bar linkage for function and path generation.

Author Contributions: Conceptualization, methodology, writing—original draft preparation, software, X.L.; data curation, writing—review and editing, software, visualization, validation J.D.; supervision, project administration C.W. All authors have read and agreed to the published version of the manuscript.

Funding: This paper is supported by the National Natural Science Foundation of China (Grant No. 52105001) and the State Key Laboratory of Robotics and Systems (HIT) (Grant No. SKLRS-2021-KF-01).

Institutional Review Board Statement: Not applicable.

Informed Consent Statement: Not applicable.

Data Availability Statement: No data available.

Conflicts of Interest: The authors declare no conflict of interest.

References

1. McCarthy, J.M.; Soh, G.S. *Geometric Design of Linkages*, 2nd ed.; Springer: New York, NY, USA, 2010.
2. Norton, R. *Design of Machinery: An Introduction to The Synthesis and Analysis of Mechanisms and Machines*, 5th ed.; McGraw-Hill: New York, NY, USA, 2011.
3. Freudenstein, F. Approximate synthesis of four-bar linkages. *Resonance* **2010**, *15*, 740–767. [[CrossRef](#)]
4. Wampler, C.W.; Morgan, A.P.; Sommese, A.J. Complete Solution of the Nine-Point Path Synthesis Problem for Four-Bar Linkages. *ASME J. Mech. Des.* **1992**, *114*, 153–159. [[CrossRef](#)]
5. Li, X.; Wei, S.; Liao, Q.; Zhang, Y. A novel analytical method for function generation synthesis of planar four-bar linkages. *Mech. Mach. Theory* **2016**, *101*, 222–235. [[CrossRef](#)]
6. Bai, S.; Angeles, J. Coupler-curve synthesis of four-bar linkages via a novel formulation. *Mech. Mach. Theory* **2015**, *94*, 177–187. [[CrossRef](#)]
7. Wu, R.; Li, R.; Bai, S. A fully analytical method for coupler-curve synthesis of planar four-bar linkages. *Mech. Mach. Theory* **2021**, *155*, 104070. [[CrossRef](#)]
8. Plecnik, M.M.; McCarthy, J.M.; Wampler, C.W. Kinematic synthesis of a Watt I six-bar linkage for body guidance. In *Advances in Robot Kinematics*; Springer: Cham, Switzerland, 2014; pp. 317–325. [[CrossRef](#)]
9. Plecnik, M.M.; McCarthy, J.M. Kinematic synthesis of stephenson iii six-bar function generators. *Mech. Mach. Theory* **2016**, *97*, 112–126. [[CrossRef](#)]
10. Plecnik, M.M.; McCarthy, J.M. Design of Stephenson linkages that guide a point along a specified trajectory. *Mech. Mach. Theory* **2016**, *96*, 38–51. [[CrossRef](#)]
11. Phukaokaew, W.; Slesongsom, S.; Panagant, N.; Bureerat, S. Synthesis of four-bar linkage motion generation using optimization algorithms. *Adv. Comput. Des.* **2019**, *4*, 197–210.
12. Sancibrian, R.; Viadero, F.; García, P.; Fernández, A. Gradient-based optimization of path synthesis problems in planar mechanisms. *Mech. Mach. Theory* **2004**, *39*, 839–856. [[CrossRef](#)]
13. Acharyya, K.; Mandal, M. Performance of EAs for four-bar linkage synthesis. *Mech. Mach. Theory* **2009**, *44*, 1784–1794. [[CrossRef](#)]
14. Penunuri, F.; Peon-Escalante, R.; Villanueva, C.; Pech-Oy, D. Synthesis of mechanisms for single and hybrid tasks using differential evolution. *Mech. Mach. Theory* **2011**, *46*, 1335–1349. [[CrossRef](#)]
15. Kiper, G.; Erez, M. Function Generation Synthesis with Planar 4-Bar Linkage as a Mixed Problem of Correlation of Crank Angles and Dead-Center Design. In *Recent Advances in Mechanisms, Transmissions and Applications. MeTrApp 2019*; Wang, D., Petuya, V., Chen, Y., Yu, S., Eds.; Mechanisms and Machine Science; Springer: Singapore, 2020; Volume 79.
16. Zhang, J.; Du, X. Time-Dependent Reliability Analysis for Function Generator Mechanisms. *ASME J. Mech. Des.* **2011**, *133*, 031005. [[CrossRef](#)]
17. Erkaya, S.; Uzmay, İ. A neural-genetic (NN-GA) approach for optimising mechanisms having joints with clearance. *Multibody Syst. Dyn.* **2008**, *20*, 69–83. [[CrossRef](#)]
18. El-Shakery, S.; Ramasan, R.; Khader, K. Analytical and graphical optimal synthesis fo crank-rocker four-bar mechanism for achieving targeted transmission angle deviations. *Jordan J. Mech. Ind. Eng.* **2020**, *14*, 303–313.

19. Daniali, H.M.; Varedi, S.M.; Dardel, M.; Fathi, A. A novel algorithm for kinematic and dynamic optimal synthesis of planar four-bar mechanisms with joint clearance. *J. Mech. Sci. Technol.* **2015**, *29*, 2059–2065. [[CrossRef](#)]
20. Bai, Z.F.; Jiang, X.; Li, F.; Zhao, J.J.; Zhao, Y. Reducing undesirable vibrations of planar linkage mechanism with joint clearance. *J. Mech. Sci. Technol.* **2018**, *32*, 559–565. [[CrossRef](#)]
21. Tian, Q.; Flores, P.; Lankarani, H.M. A comprehensive survey of the analytical, numerical and experimental methodologies for dynamics of multibody mechanical systems with clearance or imperfect joints. *Mech. Mach. Theory* **2018**, *122*, 1–57. [[CrossRef](#)]
22. Xiang, W.; Yan, S.; Wu, J.; Niu, W.; Singh, R.; Pan, Z. Dynamic response and sensitivity analysis for mechanical systems with clearance joints and parameter uncertainties using Chebyshev polynomials method. *Mech. Syst. Signal Pr.* **2020**, *138*, 106596. [[CrossRef](#)]
23. Wu, H.; Niu, W.; Wang, S.; Yan, S. An optimization method for control parameters of underwater gliders considering energy consumption and motion accuracy. *Appl. Math. Model.* **2021**, *90*, 1099–1119. [[CrossRef](#)]
24. Flores, P.; Koshy, C.S.; Lankarani, H.M.; Ambrósio, J. Numerical and experimental investigation on multibody systems with revolute clearance joints. *Nonlinear Dyn.* **2011**, *65*, 383–398. [[CrossRef](#)]
25. Wang, X.; Liu, G.; Ma, S. Dynamic analysis of planar mechanical systems with clearance joints using a new nonlinear contact force model. *J. Mech. Sci. Technol.* **2016**, *30*, 1537–1545. [[CrossRef](#)]
26. Wang, G.; Qi, Z.; Wang, J. A differential approach for modeling revolute clearance joints in planar rigid multibody systems. *Multibody Syst. Dyn.* **2017**, *39*, 311–335. [[CrossRef](#)]
27. Farahan, S.B.; Ghazavi, M.R.; Rahmanian, S. Bifurcation in a planar four-bar mechanism with revolute clearance joint. *Nonlinear Dyn.* **2017**, *87*, 955–973. [[CrossRef](#)]
28. Ebrahimi, S.; Salahshoor, E.; Moradi, S. Vibration performance evaluation of planar flexible multibody systems with joint clearance. *J. Braz. Soc. Mech. Sci. Eng.* **2017**, *39*, 4895–4909. [[CrossRef](#)]
29. Flores, P. A parametric study on the dynamic response of planar multibody systems with multiple clearance joints. *Nonlinear Dyn.* **2010**, *61*, 633–653. [[CrossRef](#)]
30. Xiang, W.; Yan, S.; Wu, J.; Gao, R.B. Complexity evaluation of nonlinear dynamic behavior of mechanisms with clearance joints by using the fractal method. *J. Mech. Eng. Sci.* **2014**, *228*, 3482–3495. [[CrossRef](#)]
31. Li, J.; Huang, H.; Yan, S.; Yang, Y. Kinematic accuracy and dynamic performance of a simple planar space deployable mechanism with joint clearance considering parameter uncertainty. *Acta Astronaut.* **2017**, *136*, 34–45. [[CrossRef](#)]
32. Xiang, W.; Yan, S. Dynamic analysis of space robot manipulator considering clearance joint and parameter uncertainty: Modeling, analysis and quantification. *Acta Astronaut.* **2020**, *169*, 158–169. [[CrossRef](#)]
33. Lai, X.; He, H.; Lai, Q.; Wang, C.; Yang, J.; Zhang, Y.; Fang, H.; Liao, S. Computational prediction and experimental validation of revolute joint clearance wear in the low-velocity planar mechanism. *Mech. Syst. Signal Pr.* **2017**, *85*, 963–976. [[CrossRef](#)]
34. Wang, G.; Wang, L. Dynamics investigation of spatial parallel mechanism considering rod flexibility and spherical joint clearance. *Mech. Mach. Theory* **2019**, *137*, 83–107. [[CrossRef](#)]
35. Liu, X.L.; Wang, C.; McCarthy, J.M. The design of coiling and uncoiling trusses using planar linkage modules. *Mech. Mach. Theory* **2020**, *151*, 103943. [[CrossRef](#)]
36. Pickard, J.K.; Carretero, J.A.; Merlet, J.P. Appropriate analysis of the four-bar linkage. *Mech. Mach. Theory* **2019**, *139*, 237–250. [[CrossRef](#)]
37. Deshpande, S.; Purwar, A. A machine learning approach to kinematic synthesis of defect-free planar four-bar linkages. *J. Comput. Inf. Sci. Eng.* **2019**, *19*, 021004. [[CrossRef](#)]
38. Liu, W.; Han, J.; Qiu, L. On the theory and methodology of systematic analysis of positions, singular configurations, branches and circuits, and ranges of motion for planar complex linkages. *Mech. Mach. Theory* **2022**, *168*, 104590. [[CrossRef](#)]
39. Lankarani, H.M.; Nikravesh, P.E. A contact force model with hysteresis damping for impact analysis of multibody systems. In Proceedings of the International Design Engineering Technical Conferences and Computers and Information in Engineering Conference, Montreal, QC, Canada, 17–21 September 1989; pp. 45–51. [[CrossRef](#)]
40. Chen, L. *Mechanical System Dynamics Analysis and ADAMS Application Tutorial*; Tsinghua University Press: Beijing, China, 2005.
41. He, X. The analysis on ADAMS dynamic simulation algorithm and parameters select. *Drive Syst. Tech.* **2005**, *19*, 27–30.
42. Archard, J.F. Contact and rubbing of flat surfaces. *J. Appl. Phys.* **1953**, *24*, 981–988. [[CrossRef](#)]
43. Fu, M.; Lei, L.; Yang, G.; Li, B. Multi-objective shape optimization of autonomous underwater glider based on fast elitist non-dominated sorting genetic algorithm. *Ocean Eng.* **2018**, *157*, 339–349. [[CrossRef](#)]
44. Sonawale, K.H.; McCarthy, J.M. Synthesis of eight-bar linkages by constraining a 6R loop. *Mech. Mach. Theory* **2016**, *105*, 337–351. [[CrossRef](#)]